 CMES, vol.103, no.4, pp.251-279, 2014

Numerical Simulation of 3D Rough Surfaces and Analysis of Interfacial Contact Characteristics

Guoqing Yang[1], Baotong Li[2,3], Yang Wang[2] and Jun Hong[2]

Abstract: Mechanical behaviors arising at the contact interface largely depend on its surface topographies, particularly when it comes to rough surfaces. A numerical simulation based on an appropriate characterization of rough surfaces especially in terms of three dimensional can be of great significance when it comes to capturing the deformation patterns of micro-scale contacts. In this paper, a simple and practical scheme is developed to generate 3D rough surfaces and to analyze and evaluate the contact characteristics. Firstly amplitude and spatial statistical characterizations of asperities are introduced to avert from the redundancy of topography data caused by traditional measuring methods. A calculation strategy is then proposed to transform varied white noise sequences into the Gaussian and non-Gaussian height sequences, in which operations like translating scaling and spatial reconfiguring are utilized to guarantee that the output first four moments are satisfied with the requirements given in advance. After that a more accurate FE model is developed to handle the problem that the asperities are so acute and tiny that can give rise to highly unstable data, in which a new meshing strategy is put forward to improve the mesh quality and solution efficiency. Finally, the simulation results are obtained through analyzing the contact characteristics of the established models. The unique feature of the proposed method is not only being capable of generating rough surfaces with any skewness and kurtosis in the whole skewness-kurtosis plane, but also narrowing down the errors of statistical characterization like the skewness and kurtosis to the level of 10^{-2} which is a highly accurate estimation in terms of the output first four moments and autocorrelation functions (ACFs). The proposed methods for numerical simulation of rough surfaces can provide massive and accurate surface topography data with a small amount of computational resources, based on which, FEM is adopted to precisely evaluate the contact

[1] College of Electromechanical Engineering, Hunan University of Science and Technology, Xiangtan 411201, Hunan, P. R. China.

[2] State Key Laboratory for Manufacturing Systems Engineering, Xi'an Jiaotong University, Xi'an 710049, P. R. China.

[3] E-mail: baotong.me@mail.xjtu.edu.cn

characteristics including load-deformation relationship, the contact pressure distribution, the real contact area and the interfacial loading/unloading characteristics, and therefore is a good choice for the study on the contact characteristics of rough surfaces.

Keywords: Surface topography, Statistical characteristics, Numerical simulation, Autocorrelation function, Power spectral density, Fast Fourier Transform.

1 Introduction

In recent decades, the study about the contact characteristics of rough surfaces on micro-scale especially in terms of three dimensional attracted great attention because it has been aware of a key factor determining the static and dynamic thermal performance of machine systems. It is proved that the numerical simulation of rough surfaces is not only a more efficient method to generate rough surfaces with the inputs determined by different height and spatial statistical parameters [Chilamakuri and Bhushan (1998)], but also an optimal method to capture the contact characteristics comprised of the load-deformation relationship, the contact pressure distribution, the real contact area and the interfacial loading/unloading characteristics of rough interfaces.

Thus far, some studies have been accomplished on generating various Gaussian and non-Gaussian rough surfaces and analyzing the contact characteristics of rough surfaces by utilizing different methods. For instance, Patir (1978) used the linear transformation of random sequence and proposed a method for generating rough surfaces with prescriptive ACFs. His scheme, however, can be impractical for its time consuming in solving a series of non-linear equations. Wu (2000) and Newland (1984) proposed numerical methods for generating Gaussian rough surfaces with applying FFT method and the prescriptive power spectral density (PSD) or ACF. Reizer (2011) simulated measured rough surfaces with Wu's and Newland's FFT methods respectively, and then conducted comparisons between the statistical characteristics of the measured and simulated rough surfaces. Watson, King, Spedding and Stout (1979) and Watson and Soedding (1982) applied time series models to simulate Gaussian and non-Gaussian engineering surfaces. Seong and Peterka (1997) and Suresh Kumar and Stathopoulos (1999) used exponential autoregressive peak generation model (EARPG) and exponential peak generation model (EPG) to find the phases for generating non-Gaussian line profiles. However, the formulas for the random phases only apply to exponential random variables, so only rough surfaces with certain skewness and kurtosis values can be generated [Wu (2004)]. According to [Hill, Hill and Holder (1976); Nagahara (2003)], non-Gaussian translator systems have been developed to generate non-Gaussian rough surfaces. Be-

sides, Wu (2004) defined one-dimensional phase sequences to generate updated white noise and non-Gaussian height sequences, which provides a basis for the generation of the 2D phase sequences in this study to make the average ACFs of the simulated rough surfaces coincide well with the input ones. As for the specific simulation process, Greenwood and Williams (1966) simplified the process by using the frictionless contact of an elastic hemisphere and a rigid flat plane to stochastically model an entire contacting surface with a postulated Gaussian height distribution. The aforementioned GW model assumed that the asperities of the surfaces deformed independently and the substrate below the asperities did not deform at all. Supplementing the GW model, many elasto-plastic asperity models have been devised [Chang, Etsion and Bogy (1987); Majumdar and Bhushan (1991); Jackson and Green (2006)]. Meanwhile, the asperity interactions were considered in [Zhao and Chang (2001); Gao, Bower, Kim, Lev and Cheng (2006); Ciavarella, Greenwood and Paggi (2008); Buczkowski and Kleiber (2009)] where the asperities were simplified geometrically for normal contact and the contact of two rough surfaces was also simplified to the contact between one rough surface and one smooth rigid plane. Although these above models have been proven feasible, most of them were proposed based on many assumptions and simplifications of the shape, magnitude and height distribution of asperities, which can limit their applications and affect the solution accuracies to some extent. Thus, to solve this problem, Jackson and Green (2005) proposed a 2D axisymmetric FE model of an elastic-perfectly plastic hemisphere in contact with a rigid flat surface. Admittedly, FEM is an effective way to overcome the defects of other analytical methods, but it calls a great challenge to control mesh quality and solution efficiency. Sahoo and Ghosh (2007) and Hyun, Pei, Molinari and Robbins (2004) simulated the interface of one rigid smooth plane and one self-affine rough surface based on fractal theory. However, there are disputes concerning whether the fractal theory can adapt to generate any engineering rough surface. Meanwhile, the above simplification of the interface may not reveal the true contact characteristics perfectly.

In this study, a simple and practical scheme is proposed to accurately generate Gaussian and non-Gaussian rough surfaces and comprehensively analyze the contact characteristics of rough surfaces. In the first section, rather than traditional measuring methods where the collected data are inaccurate and redundancy due to the measuring equipment and the choice of measuring area, the statistical characteristics consisted of amplitude and spatial characterization parameters are utilized here to effectively capture the detailed surface topography data [Wu (2000); Wu (2004); Bakolas (2003)]. Next, the FFT method is adopted in the simulation process to improve the calculation efficiency since it is relatively faster and more convenient when compared with time series tool as a common used method. Be-

sides, another calculation strategy is also proposed for generating non-Gaussian sequences directly from white noise sequences with the input statistical parameters and ACFs. More than that, this strategy is not only able to generate rough surfaces with any skewness and kurtosis in the whole skewness-kurtosis plane, but also narrow down the errors generated during the filter process by eliminating this complicated procedure, which is a great improvement over the previous methods. In addition, after the generation of non-Gaussian rough surfaces, array restructure and rearrangement methods, substituting for the conventional intricate linear transformation and filter process aimed to remain the satisfied first four moments unchanged, are introduced to ensure that the generated Gaussian and non-Gaussian rough surfaces have almost the same ACFs with the input ones. Last but not the least, based on the simulated models, the quantitative study, more than the qualitative study, is also carried on through FEM about the contact characteristics, such as load-deformation relationship, the contact pressure distribution, the real contact area and the interfacial loading/unloading characteristics, to reveal the superiority of the proposed models as well as lay a solid foundation for further study on surface topography optimization.

2 Numerical simulation of rough surfaces

2.1 Statistical characteristics

The surface topographies of rough interfaces on micro-scale are so irregular that can only be well described by the statistical characteristics of which the parameters are calculated with references to the height distribution, probability density function (PDF), power spectral density (PSD) or the autocorrelation function (ACF).

2.1.1 Amplitude characterization

Height distribution function and the corresponding PDF play an important part in deciding most of the statistical height parameters of rough surfaces. In most cases, Gaussian distribution is assumed for simplification, but in fact, most machined rough surfaces are non-Gaussian [Watson, King, Spedding and Stout (1979)]. For a surface described by a continuous univariate PDF $f(z)$, the v^{th} central moment u_v could be expressed as follows:

$$u_v = \mathrm{E}\left((z-\bar{z})^v\right) = \int_{-\infty}^{+\infty} (z-\bar{z})^v f(z) dz \tag{1}$$

where E is the expectation operator; $\bar{z}$ is the average height of the rough surface. Generally speaking, $\bar{z}$ is defined to be zero at the beginning of numerical simulation, and finally modified to the input mean value μ by adding μ to the height sequence

z.

$$\bar{z} = \mathrm{E}(z) = \int_{-\infty}^{+\infty} z f(z) dz \tag{2}$$

According to Eq. (3) and Eq. (4), the first central moment u_1 is zero; the second one is equal to the variance σ^2, where σ is the standard deviation of the height sequence z; When $v \geq 3$, the v^{th} central moment u_v can also be standardized through being divided by σ^v, especially, the skewness and kurtosis are defined to be the 3^{rd} and 4^{th} standard moments, respectively.

$$S_{kz} = \frac{u_3}{\sigma^3}, \quad K_{uz} = \frac{u_4}{\sigma^4} \tag{3}$$

For a rough surface described by a discrete height sequence $z(m, n)$, the v^{th} central moment u_v is as follows:

$$u_v = \mathrm{E}\left((z - \bar{z})^v\right) = \sum_{k=0}^{m-1} \sum_{l=0}^{n-1} \frac{(z_{k,l} - \bar{z})^v}{mn} \tag{4}$$

To sum up, the first four standard moments can be described as follows:

$$\mu = \sum_{k=0}^{m-1} \sum_{l=0}^{n-1} \frac{z_{k,l}}{mn} \tag{5}$$

$$\sigma = \sqrt{\sum_{k=0}^{m-1} \sum_{l=0}^{n-1} \frac{(z_{k,l} - \mu)^2}{mn}} \tag{6}$$

$$S_{kz} = \sum_{k=0}^{m-1} \sum_{l=0}^{n-1} \frac{(z_{k,l} - \mu)^3}{mn \cdot \sigma^3} \tag{7}$$

$$K_{uz} = \sum_{k=0}^{m-1} \sum_{l=0}^{n-1} \frac{(z_{k,l} - \mu)^4}{mn \cdot \sigma^4} \tag{8}$$

where m and n stand for the numbers of row and column, respectively. When z has a mean of zero and a variance of 1, S_{kz} and K_{uz} are equivalent to the 3^{rd} and 4^{th} original moments, respectively.

2.1.2 Spatial characterization

The statistical parameters of spatial characteristics are mainly determined by ACF or PSD, and the PSD can be obtained from the ACF function with fast Fourier

transform (FFT) method. For a continuous height function $z(x, y)$, the normalized ACF can be described as follows:

$$R(\tau_x, \tau_y) = \frac{\int_0^{L_x-\tau_x}\int_0^{L_y-\tau_y} z(x,y)z(x+\tau_x, y+\tau_y)dxdy}{(L_x-\tau_x)(L_y-\tau_y)\sigma^2} \tag{9}$$

where L_x and L_y are the lengths of rough surface in x and y directions, respectively; τ_x and τ_y are the distance in x and y directions between any two points in sample area with τ_x=$Z(0\sim(m\text{-}1))\Delta x$, τ_y=$Z(0\sim(n\text{-}1))\Delta y$; $z(x,y)$ is defined as a discrete sequence with spacing of $\Delta x = \Delta y$=1μm and when m and n approach ∞, the corresponding ACF can be expressed as Eq. (10), especially $R(0,0)$=σ^2.

$$R(k,l) = \sum_{I=1}^{m-k}\sum_{J=1}^{n-l} \frac{z(I,J)z(k+I,l+J)}{(m-k)(n-l)} \tag{10}$$

where k=0, 1, 2, …, m-1; l=0, 1, 2, …, n-1.

Nowadays, PSD has become a widely accepted method for characterizing the spatial frequencies of rough surfaces which can provide spectrum features of spatial frequencies and contains the information about spatial frequencies from 0 to ∞ (frequencies 0 and ∞ stand for the surfaces of infinite flat and ones with infinite small asperities, respectively). In this study, the PSD can be derived from the height information (continuous height distribution function $z(x, y)$ or discrete height sequence $z(m, n)$) or the ACF of rough surfaces with FFT method as Eq. (11) or Eq.(12).

$$P(f_r, f_s) = \frac{1}{mn}\left|\sum_{k=0}^{m-1}\sum_{l=0}^{n-1} z(k,l)\exp\left[-2\pi i\left(\frac{kr}{m}+\frac{ls}{n}\right)\right]\right| \tag{11}$$

$$P(f_r, f_s) = \left|\sum_{k=0}^{m-1}\sum_{l=0}^{n-1} R(k,l)\exp\left[-2\pi i\left(\frac{kr}{m}+\frac{ls}{n}\right)\right]\right| \tag{12}$$

where r=0, 1, …, m-1, s=0, 1, …, n-1; f_x and f_y stand for the frequencies in x and y directions with $f_x = r/(m\Delta x)$, $f_y = s/(n\Delta y)$.

2.2 Simulations of Gaussian rough surfaces

As shown in Fig.1, the simulation of Gaussian rough surfaces is the process of producing 2D phase sequences from white noise sequences and then updating for generating Gaussian rough surfaces. In order to make the target Gaussian rough surfaces satisfy the input ACF, μ, σ, S_{kz} and K_{uz}, the discrete method for the input ACFs and the definition of phase sequences as well as the computation of the PSD constants of white noise sequences are presented in detail. The concrete steps for the simulation of Gaussian rough surfaces are listed as follows:

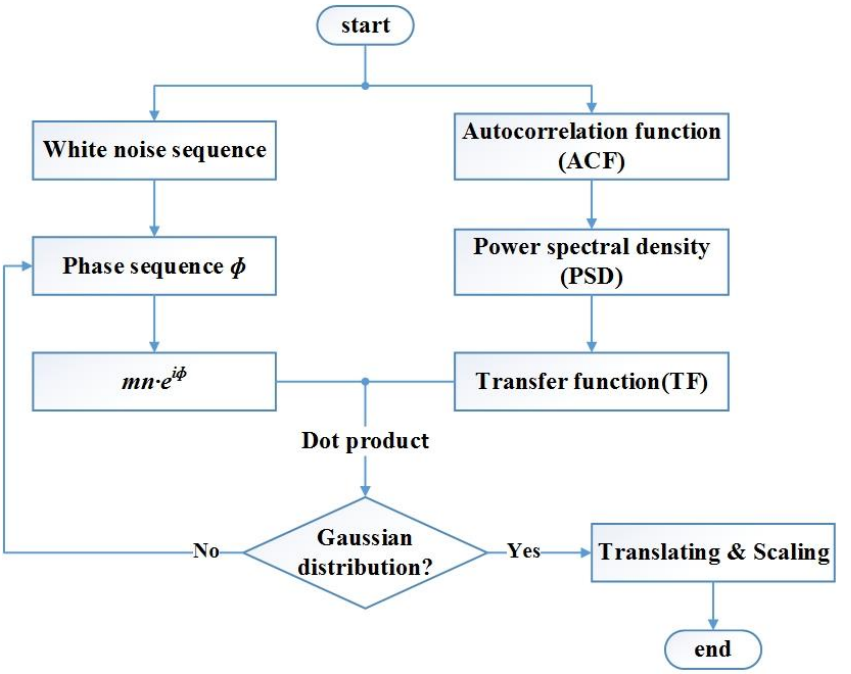

Figure 1: Numerical simulation of Gaussian rough surfaces.

1. The discrete form of ACF $R(m, n)$ is extracted from the given ACF $f(x, y)$.

(1) The input ACF should be defined at first. For example, the following exponential form of ACF $f(x, y)$ is widely quoted.

$$f(x,y) = \sigma^2 \exp\left[-2.3\sqrt{\left(\frac{x'}{\beta_x}\right)^2 + \left(\frac{y'}{\beta_y}\right)^2}\right] \tag{13}$$

$$x' = x\cos\phi + y\sin\phi, \quad y' = -x\sin\phi + y\cos\phi$$

where σ is the standard deviation of height sequence; β_x and β_y stand for the autocorrelation lengths in x and y directions, respectively; ϕ stands for the prescriptive orientation of surface texture.

(2)An equal discrete spacing in x and y directions needs to be specified (for example, $\Delta x = \Delta y$=1μm) and then, discretize the given ACF into sequence $R(m+1, n+1)$ within the range of -m/2$\leq x \leq m$/2 and -n/2$\leq y \leq n$/2.

$$R(g + \frac{m}{2} + 1, h + \frac{n}{2} + 1) = f(g,h) \tag{14}$$

where m and n are numbers of surface points in x and y directions; g=-m/2, -m/2+1, …, m/2; h=-n/2, -n/2+1, …, n/2.

(3) One of the repeated rows m/2+1 or m/2+2, and the repeated columns n/2+1or n/2+2 in the sequence $R(m+1, n+1)$ is required to be deleted to generate the sequence $R(m, n)$ of the same size with the target rough surface.

2. The PSD and TF can be obtained from $R(m, n)$.

(1) FFT method is applied here to get the PSD $P(I, J)$ according to Eq. (12).

(2) Since the PSD of white noise is a constant C, assuming C=1, the transfer function H (m, n) can be obtained:

$$H = \sqrt{\frac{P}{C}} = \sqrt{P} \tag{15}$$

3. The phase sequence $\Phi(m, n)$ can be produced from the white noise sequence η (m, n) which needs to be updated with inverse fast Fourier transform (IFFT) method.

(1) The white noise generator randn(m, n) is used to obtain the white noise sequence η (m, n).

(2) The phase sequence $\Phi(m, n)$ is generated from the sequence $\eta(m, n)$ with Eq. (16).

$$\Phi(k+1,l+1) = 2\tan^{-1}\left(\frac{-\sum_{r=0}^{m-1}\sum_{s=0}^{n-1}\eta(r+1,s+1)\sin(\frac{2\pi kr}{m}+\frac{2\pi ls}{n})}{\sum_{r=0}^{m-1}\sum_{s=0}^{n-1}\eta(r+1,s+1)\cos(\frac{2\pi kr}{m}+\frac{2\pi ls}{n})}\right) \tag{16}$$

where all the elements in the phase sequence Φ range from 0 to 2π, and the computation of $\Phi(m, n)$ can be conducted with FFT method to improve the efficiency.

(3) The white noise sequence $\eta(m, n)$ is updated from $\Phi(m, n)$ with IFFT method:

$$\eta(k+1,l+1) = \sum_{r=0}^{m-1}\sum_{s=0}^{n-1}\exp\left(i\Phi + \frac{2\pi ikr}{m} + \frac{2\pi ils}{n}\right) \tag{17}$$

(4) FFT method is then introduced to the updated the white noise sequence $\eta(m, n)$.

$$A(k+1,l+1) = \sum_{r=0}^{m-1}\sum_{s=0}^{n-1}\eta(r+1,s+1)e^{-2\pi i(kr/m+ls/n)} \approx mn\cdot e^{\mathrm{i}\Phi} \tag{18}$$

4. The Gaussian sequence $z_0(m, n)$ is generated from the dot-product of A and H with IFFT method.

$$z_0(k+1,l+1) = \frac{1}{mn}\sum_{r=0}^{m-1}\sum_{s=0}^{n-1}(A\cdot H)e^{2\pi i(kr/m+ls/n)} \tag{19}$$

5. Repeat steps 3∼4, if the skewness and kurtosis values of z_0 approach 0 and 3, respectively, otherwise, repeat the step 2.

6. The Gaussian sequence $z_0$is required to be scaled and translated to obtain the target Gaussian height sequence.

(1) According to Eq. (2), the mean μ_0 and standard deviation σ_0 of z_0 can be calculated.

(2) The sequence z_0 is scaled to $z_1(z_1{=}\sigma{\cdot}z_0/\sigma_0)$ whose standard deviation is equal to σ. At the same time, the PSD (equal to the constant C) of the updated white noise sequence as well as H can be updated: $C{=}(\sigma_0/\sigma)^2$ and $H = P^{0.5}(\sigma/\sigma_0)$.

(3) The height sequence z_1 is translated in the height direction: $z_G = z_1\text{-}\mu_0{+}\mu$, to obtain the target Gaussian sequence z_G with the mean of μ and the standard deviation of σ.

The Gaussian rough surfaces produced with aforementioned simulation method are able to meet the requirements of the height statistical characteristics and ACFs, and moreover, can provide the spatial distribution rules for the corresponding non-Gaussian ones investigated in the following section..

2.3 Simulations of non-Gaussian rough surfaces

There are usually two steps in the simulation of target non-Gaussian rough surfaces including the non-Gaussian transformation and the linear transformation [Wu (2004); Hill, Hill and Holder (1976); Nagahara (2003); Hu and Tonder (1992); Bakolas (2003)] Non-Gaussian height sequences are produced through non-Gaussian transformation with the transitional skewness $S_{k\eta}$ and kurtosis $K_{u\eta}$ determined from Eq. (20), and subsequently filtered to satisfy the input first four moments and ACFs.

$$\begin{cases} S_{k\eta} = \dfrac{\left(\sum_{i=1}^{m\cdot n}\theta_i^2\right)^{3/2}}{\sum_{i=1}^{m\cdot n}\theta_i^3}S_{kz} \\ K_{u\eta} = \dfrac{K_{uz}\left(\sum_{i=1}^{m\cdot n}\theta_i^2\right)^2 - 6\sum_{i=1}^{m\cdot n-1}\sum_{i=j+1}^{m\cdot n}\theta_i^2\theta_j^2}{\sum_{i=1}^{m\cdot n}\theta_i^4} \end{cases} \tag{20}$$

where S_{kz} and K_{uz} are the input skewness and kurtosis values; $\theta_i = h(k, l)$ where $h(k, l)$, working as the filter coefficient, can be obtained from the transfer function

(TF), and k=1, 2, …, m, l=1, 2, …, n as well as i=(k-1)$m+l$. Because the calculation of the summation of $\theta_i^2 \cdot \theta_j^2$ items is too time consuming, Bakolas (2003) simplified the above computation of the kurtosis from Eq. (21) to Eq. (22)

$$\sum_{i=1}^{m\cdot n-1} \sum_{j=i+1}^{m\cdot n} \theta_i^2 \theta_j^2 = \frac{1}{2}\left(\left(\sum_{i=1}^{m\cdot n} \theta_i^2\right)^2 - \sum_{i=1}^{m\cdot n} \theta_i^4\right) \tag{21}$$

$$K_{u\eta} = \frac{(\sum_{i=1}^{m\cdot n} \theta_i^2)^2}{\sum_{i=1}^{m\cdot n} \theta_i^4}(K_{uz}-3)+3 \tag{22}$$

Although S_{kz} and K_{uz} are within the whole skewness-kurtosis plane ($K_{uz} - S_{kz}^2 - 1 \geq 0$), the linear transformation as shown in Eq. (20) may enable $S_{k\eta}$ and $K_{u\eta}$ to deviate from the corresponding skewness-kurtosis plane: $K_{u\eta} - S_{k\eta}^2 - 1 \geq 0$. So the method for generating non-Gaussian rough surfaces cannot cover the whole skewness-kurtosis plane.

In this end, an optimal non-Gaussian translator system is introduced in this section to transform varied white noise sequences directly into non-Gaussian height sequences with the accurate input first four moments as shown in Fig.2. The transformed sequences, however, are completely disorganized and that's why the reconfiguration is an indispensable procedure for generating the target non-Gaussian height sequences with the prescriptive ACF according to the spatial distribution characteristics of the corresponding Gaussian rough surfaces.

2.3.1 Choice of non-Gaussian translator systems

Nowadays, two non-Gaussian transformation methods, Johnson's and Pearson's translator systems, are accepted by most academics. Both of them can achieve the aim of generating the sequences of height distributions covering the whole skewness-kurtosis plane: $K_{uz} - S_{kz}^2 - 1 \geq 0$ but only one of them will be utilized here to generate non-Gaussian sequences in the terms of transformation accuracy and efficiency. Johnson system transforms a random Gaussian sequence to a non-Gaussian sequence with given mean, standard deviation, skewness and kurtosis by using three types of fitting methods, S_B, S_U and S_L.

The lognormal distribution S_L:

$$z_2 = \xi + \lambda e^{(\eta-\gamma)/\delta} \qquad (\xi < \eta) \tag{23}$$

The bounded distribution S_B:

$$z_2 = \xi + \frac{\lambda \exp^{(\eta-\gamma)/\delta}}{1+e^{(\eta-\gamma)/\delta}} \qquad (\xi < \eta < \xi+\lambda) \tag{24}$$

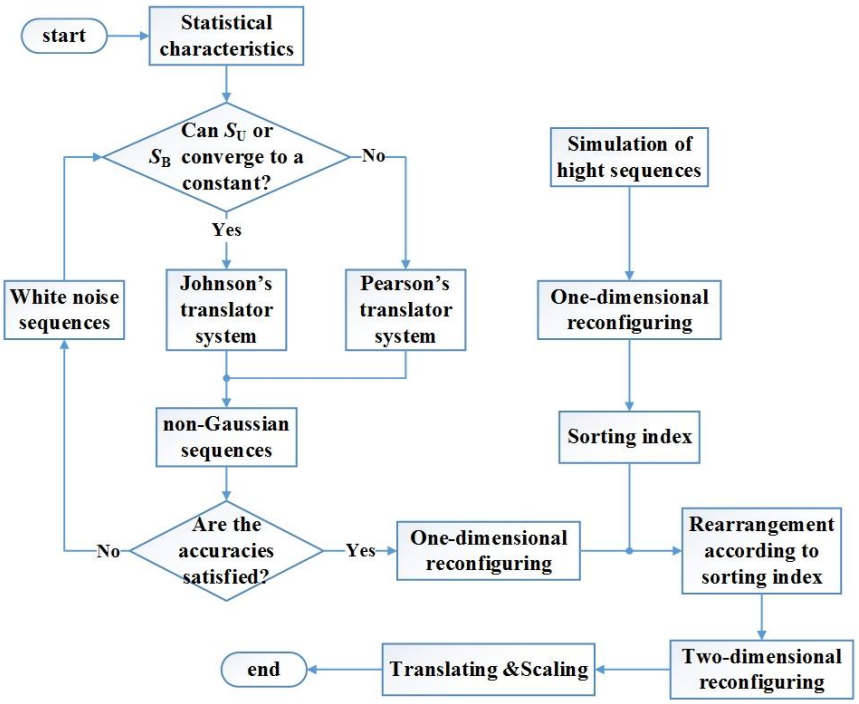

Figure 2: Numerical simulation of non-Gaussian rough surfaces.

The unbounded distribution S_U:

$$z_2 = \xi + \lambda \sinh \frac{\eta - \gamma}{\delta} \tag{25}$$

where η is the white noise sequence and z_2 is the non-Gaussian sequence; γ and δ are shape parameters; λ and ξ are proportional coefficient and position parameter, respectively. The value of all the parameters including γ, δ, λ and ξ can be determined by the given skewness and kurtosis. Through the transformation, any non-Gaussian rough surface with given skewness and kurtosis can be obtained.

Johnson's translator system tends to use the S_L method when neither S_U nor S_B can converge to a constant, which may give rise to the reduction of transformation accuracy. Pearson's non-Gaussian translator system of frequency curves uses a probability function $p(x)$ satisfying the following differential equation Eq. (26):

$$\frac{d(\log p(x))}{dx} = -\frac{a+x}{c_0 + c_1 x + c_2 x^2} \tag{26}$$

where a, c_0, c_1 and c_2 are constants that can be obtained with given standard de-

viation, skewness, kurtosis and the probability function derived from the above differential equation.

Pearson's system introduces some widely used distributions including gamma, beta, F-distribution, t-distribution and so on to ensure that their first four moments coincide well with the prescriptive ones. However, its utility is limited because the PDF to be used must be chosen from the aforementioned distribution functions [Bakolas (2003)]. In this study, Johnson's translator system is given the priority to be considered first during the simulation of non-Gaussian rough surfaces. Nevertheless, when S_U and S_B in Johnson's translator system are unable to converge, Pearson's translator system will take the place to improve the accuracy and efficiency of non-Gaussian transformation.

2.3.2 Non-Gaussian transformation

Johnson's or Pearson's translator system can directly transform Gaussian or white noise sequences to non-Gaussian sequences, respectively, with given values of μ, σ, S_{kz} and K_{uz}. In this study, the complicated filter process is eliminated and height sequences with any input S_{kz} and K_{uz} in the whole skewness-kurtosis plane ($K_{uz} - S_{kz}^2 - 1 \geq 0$) can be obtained by carrying out the following steps.

1. The white noise generator randn(m,n) is utilized to obtain the white noise sequence $\eta\ (m, n)$ and transform it to a non-Gaussian sequence $z_2(m, n)$ with Johnson's translator system in terms of the input first four moments; If S_B or S_U are unable to converge, use the Pearson's translator system to obtain the non-Gaussian sequence $z_2\ (m, n)$, instead.

2. The skewness and kurtosis of the sequence $z_2\ (m, n)$ is calculated according to Eq.(7) and Eq. (8) and repeat steps 1$\sim$3 if the accuracy cannot meet the satisfaction.

3. The sequence $z_2(m, n)$ needs to be scaled and translated with z_3=$\sigma \cdot z_2/\sigma_1$-$\mu_1$+$\mu$ (σ_1 and μ_1 stand for the standard deviation and the mean of the sequence z_2) to update the non-Gaussian sequence to satisfy the given first four moments.

As mentioned above, non-Gaussian height sequences can be transformed from white noise sequences conforming strictly to the input first four moments. The accuracies of the skewness and kurtosis can be improved by the circulation of transformation process and the mean and standard deviation can be strictly guaranteed by the translating and scaling methods. After the aforementioned non-Gaussian transformation, the non-Gaussian height sequences with given height statistical characteristics will be generated.

2.3.3 Restructure and rearrangement of the height sequences

The above section generates the non-Gaussian sequence z_3 (m, n) whose first four moments accurately approach those of the target height sequence. Afterwards, the restructure and rearrangement methods of height sequences are utilized to make the target non-Gaussian height sequence satisfy the given ACFs in x and y directions on the basis of the spatial distribution of the corresponding Gaussian rough surfaces. The following steps can be adopted:

1. The simulated Gaussian sequence z_G (m, n) and the non-Gaussian sequence $z_3(m, n)$ need to be restructured into sequences $q(m \cdot n, 1)$ and $Q(m \cdot n, 1)$, respectively.

2. The sorting and indexing tools in Matlab are introduced to arrange the sequence $q(m \cdot n, 1)$ and Q($m \cdot n$, 1) then, rearrange the sequence Q($m \cdot n$, 1) in terms of the sorting index of the sequence $q(m \cdot n, 1)$.

3. The rearranged sequence Q($m \cdot n$, 1) is required to get restructured into the target non-Gaussian height sequence $z_N(m, n)$ which has almost the same ACFs with those of the corresponding Gaussian height sequence z_G.

The proposed restructure and rearrangement methods, substituting for the conventional complicated linear transformation and filter process to remain the satisfied first four moments unchanged, will make the generated Gaussian and non-Gaussian rough surfaces have nearly the same ACFs with the input ones. So the non-Gaussian rough surfaces with the prescriptive first four moments and ACFs could be accurately simulated.

2.4 Simulation cases

Both of Gaussian and non-Gaussian rough surfaces have isotropic and anisotropic, geometrical and physical characteristics. As shown in Fig.3 and Fig.4, the simulated isotropic Gaussian and non-Gaussian rough surfaces as well as the anisotropic ones are obtained. It is obvious that isotropic rough surfaces have the same autocorrelation lengths with each other while anisotropic rough surfaces have different autocorrelation lengths in x and y directions. The simulation time of GS 1-1, NGS 1-2, GS 2-1, NGS 2-2, GS 3-1, NGS 3-2, GS 4-1 and NGS 4-2 are 0.7, 0.8, 0.5, 1.3, 2.5, 3.3, 2.6 and 3.3 seconds, respectively. Especially, it has been noticed that decreasing the discrete point count or the accuracy requirements of the skewness and kurtosis values means less time to simulate the rough surfaces with the same statistical parameters.

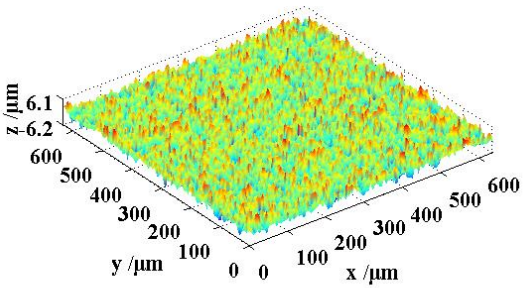

(a) GS 1-1: 128×128, $\beta_x=\beta_y=10$, $\Delta x=\Delta y=5$, $R_q=1.6$, $R_a=1.27$ /μm

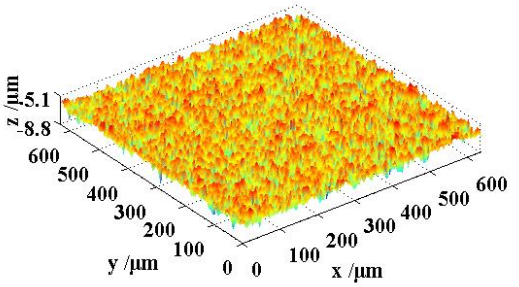

(b) NGS 1-2: 128×128, $S_{kz}=-0.5$, $K_{uz}=3.5$, $\beta_x=\beta_y=10$, $\Delta x=\Delta y=5$, $R_q=1.6$, $R_a=1.27$ /μm

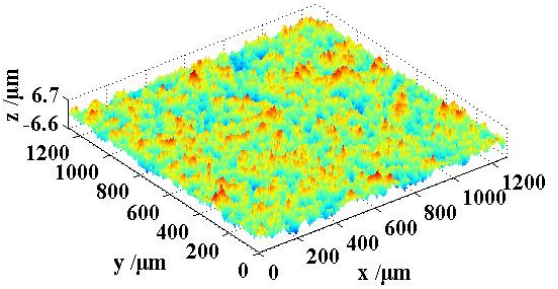

(c) GS 2-1: 256×256, $\beta_x=\beta_y=50$, $\Delta x=\Delta y=5$, $R_q=1.6$, $R_a=1.28$ /μm

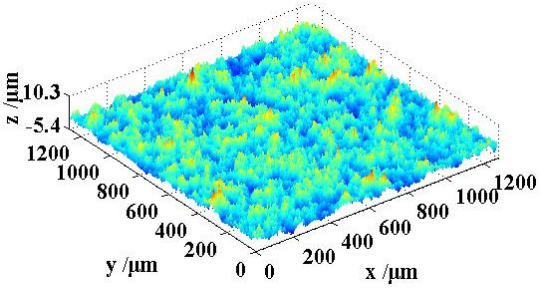

(d) NGS 2-2: 256×256, $S_{kz}=0.5$, $K_{uz}=3.5$, $\beta_x=\beta_y=50$, $\Delta x=\Delta y=5$, $R_q=1.6$, $R_a=1.26$ /μm

Figure 3: Isotropic Gaussian and non-Gaussian rough surfaces.

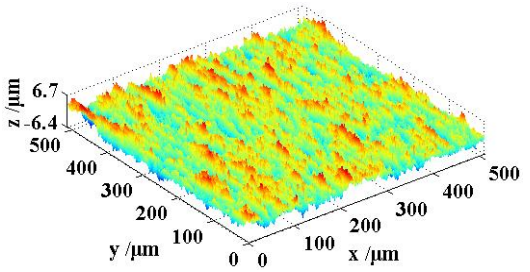

(a) GS 3-1: 512×512, β_x=10, β_y=50, Δx=Δy=1, R_q=1.6, R_a=1.28 /μm

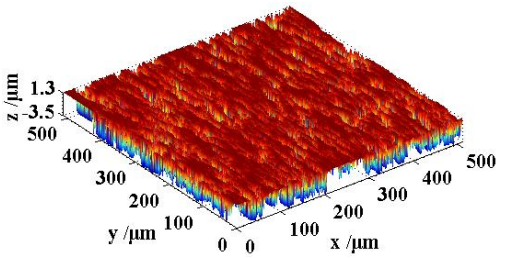

(b) NGS 3-2: 512×512, S_{kz}=-1, K_{uz}=2.5, β_x=10, β_y=50, Δx=Δy=1, R_q=1.6, R_a=1.36 /μm

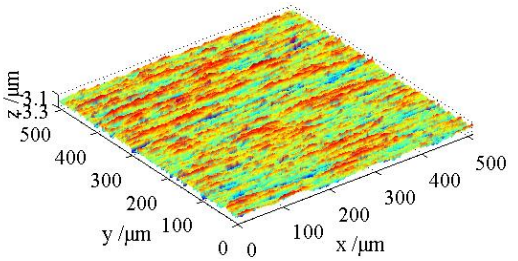

(c) GS 4-1: 512×512, $_x$=100, β_y=5, Δx=Δy=1, R_q=0.8, R_a=0.614 /μm

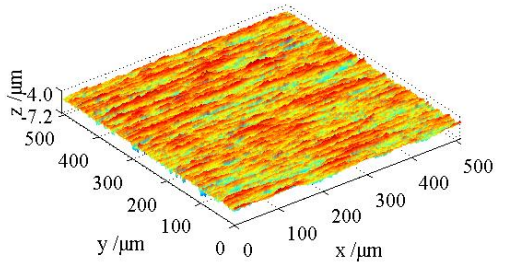

(d) NGS 4-2: 512×512, S_{kz}=-0.5, K_{uz}=4.5, $_x$=100, β_y=5, Δx=Δy=1, R_q=0.8, R_a=0.638 /μm

Figure 4: Anisotropic Gaussian and non-Gaussian rough surfaces.

2.4.1 Statistical height characteristics

The height distribution characteristics of the first group rough surfaces (GS 1-1 and NGS 1-2) are shown in Fig. 5 where the normal distribution plot indicates that NGS 1-2 has a clear deviation from the linear normal distribution. Similarly, the height distributions of the other simulated non-Gaussian rough surfaces can be obtained as shown in Fig. 6 where it is obvious that the probability distribution of the rough surfaces with negative skewness skew to negative side of the normalized height, and vice versa.

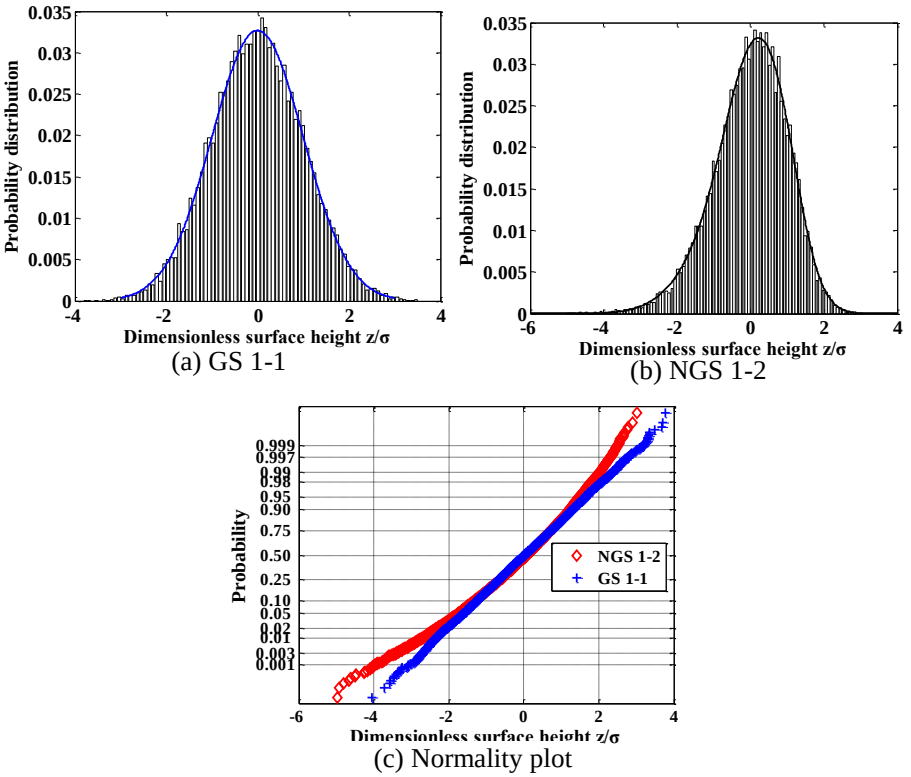

Figure 5: Height distribution characteristics of GS 1-1 and NGS 1-2.

As common used roughness parameters, the profile arithmetic mean R_a and the root-mean-square (rms) roughness R_q (especially, R_q=σ) are calculated. As shown in Fig. 3 and Fig.4, the ratio of R_a to R_q of Gaussian rough surfaces approximately equals 0.8 while that of non-Gaussian rough surfaces deviates from 0.8. As for the accuracies of the first four moments, μ and σ can be kept consistent with the

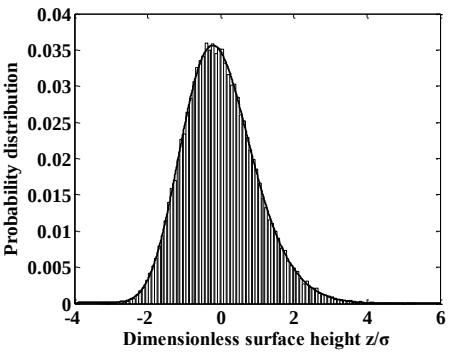

(a) NGS 2-2

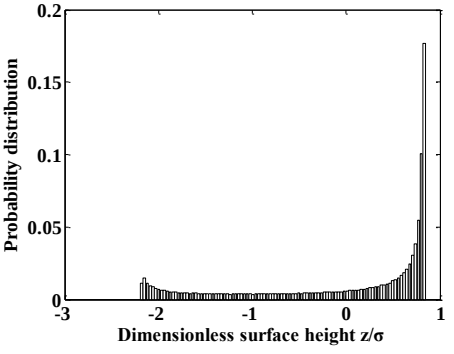

(b) NGS 3-2

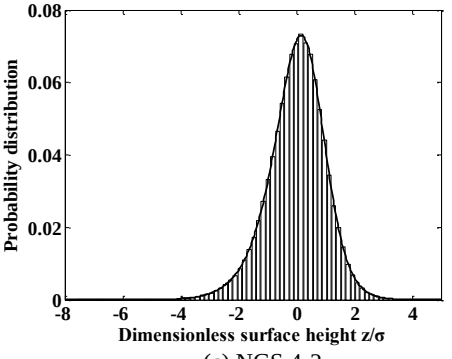

(c) NGS 4-2

Figure 6: Height distributions of other non-Gaussian surfaces.

Table 1: Errors of the skewness and kurtosis values.

Rough surfaces	Skewness			Kurtosis		
	input	output	error	input	output	error
GS 1-1	0	-0.009	-0.009	3	3.027	0.027/0.9%
GS 2-1		0.003	0.003		2.99	0.010/0.3%
GS 3-1		0.010	0.010		2.973	-0.027/0.9%
GS 4-1		-0.004	-0.004		2.98	0.02/0.7%
NGS 1-2	-0.5	-0.496	0.004/0.8%	3.5	3.485	0.015/0.4%
NGS 2-2	0.5	0.498	0.002/0.4%	3.5	3.508	0.008/0.2%
NGS 3-2	-1.0	-1.001	-0.001/0.1%	2.5	2.502	0.002/0.1%
NGS 4-2	-0.5	-0.502	-0.002/0.4%	4.5	4.46	0.040/0.9%

output ones by the scaling and translating methods and the errors of the skewness and kurtosis values listed in Table 1 can be reduced sharply by the elimination of filter process.

The results show that the skewness and kurtosis errors are less than 0.03 and 0.05, respectively. Comapred with the results in [Reizer (2011)], the accuracy of the skewness and kurtosis values is greatly improved. Moreover, with more time given to simulation, the accuracy of the skewness and kurtosis values could be further improved.

2.4.2 *ACFs of rough surfaces*

The normalized average ACFs of the simulated rough surfaces in x and y directions are extracted from the spatial characteristics based on the method with reference to [Wu (2004)]. As shown in Fig.7 and Fig.8, the ACFs of the non-Gaussian rough surfaces coincide well with those of the corresponding Gaussian rough surfaces. What's more, it can also be found that when $m \cdot \Delta x/\beta_x \geq 20$ or $n \cdot \Delta y/\beta_y \geq 20$, the ACFs of simulated rough surfaces in x or y direction agree with the corresponding theoretical ones.

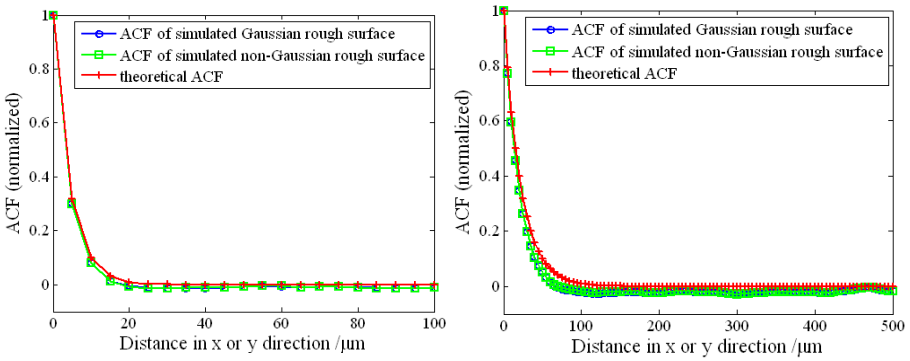

(a) GS 1-1 and NGS 1-2 (b) GS 2-1 and NGS 2-2

Figure 7: ACFs of isotropic group surfaces in x or y directions.

2.4.3 *Level-spacing distribution of asperities*

Eight-point method is introduced in this section to find the asperity peaks and valleys of rough surfaces. Specifically speaking, a point $K_{i,j}$ in a rough surface can be found surrounded by eight points as shown in Fig.9. Once the height coordinate of point $K_{i,j}$ is larger or smaller than those of the eight surrounding points, the point $K_{i,j}$ can be taken as an asperity peak or valley. Thus, based on the eight-point

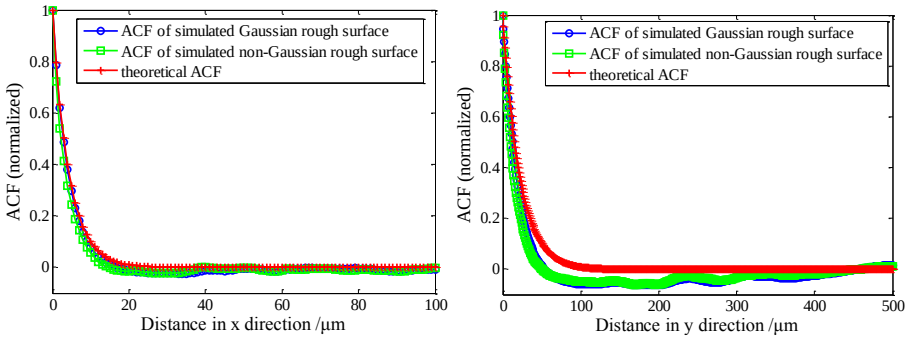

(a) GS 3-1 and NGS 3-2 (b) GS 4-1 and NGS 4-2

Figure 8: ACFs of anisotropic group surfaces in x and y directions.

method, all of the asperity peaks and valleys of simulated non-Gaussian rough surfaces could be found out as shown in Fig.10 where "+" and "o" stand for the peaks and the valleys, respectively. Meanwhile, the spacing characteristics of asperity peaks in x and y directions are extracted as shown in Table 2. Moreover, the spacing distribution of the asperity peaks and valleys can be adjusted by the discrete spacing (Δx and Δy) and the corresponding autocorrelation length in x and y directions (β_x and β_y).

Table 2: Spacing characteristics of asperity peaks.

Rough surfaces	Mean spacing / μm		Spacing range / μm	
	x-dir	y-dir	x-dir	y-dir
NGS 1-2	48.7	50.6	26.9∼165	30.6∼267.5.
NGS 2-2	69.5	69.3	37.5∼153.1	42.8∼150
NGS 3-2	14.3	13.9	30.6∼98	6∼184
NGS 4-2	21.1	24.7	8.2∼114.5	16∼46.5

2.4.4 Texture direction of rough surface

The proposed scheme is suitable for generating Gaussian and non-Gaussian rough surfaces with isotropic and linear anisotropic surface texture. Among the anisotropic rough surfaces, as shown in Fig. 4, GS 3-1 and NGS 3-2 with ϕ=0 and $\beta_x < \beta_y$ present longitudinal surface texture, while GS 4-1 and NGS 4-2 with ϕ=0 and $\beta_x > \beta_y$ show obvious transverse surface texture. If the orientation angle ϕ of

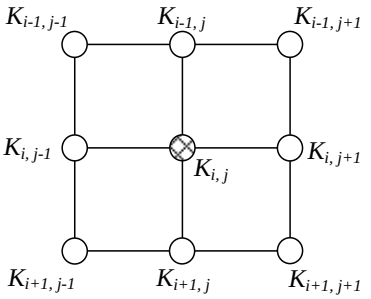

Figure 9: Eight-point method for peaks and valleys.

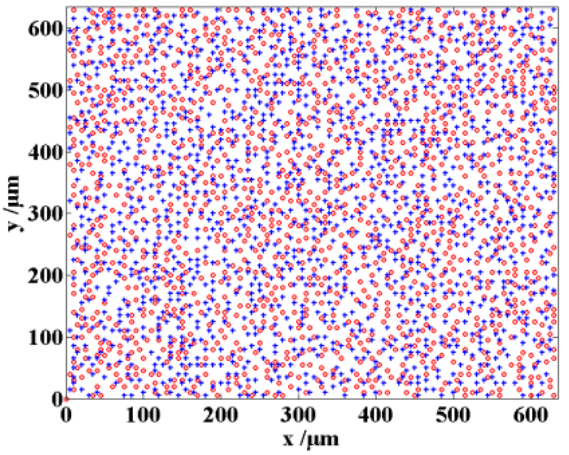

Figure 10: Asperity peaks "+" and valleys "o" of NGS 1-2.

the rough surface NGS 4-2 is changed from 0 to 45° or 120°, considering that the orientation angle ϕ equals the rotation angle of z axis, the corresponding surfaces will be generated as shown in Fig. 11.

Using the aforementioned simulation method, Gaussian and non-Gaussian rough surfaces can be generated with any skewness and kurtosis values in the whole skewness-kurtosis plane ($K_{uz} - S_{kz}^2 - 1 \geq 0$) which help lay a solid foundation for the following section about the study of the contact characteristics of two non-Gussian surfaceas.

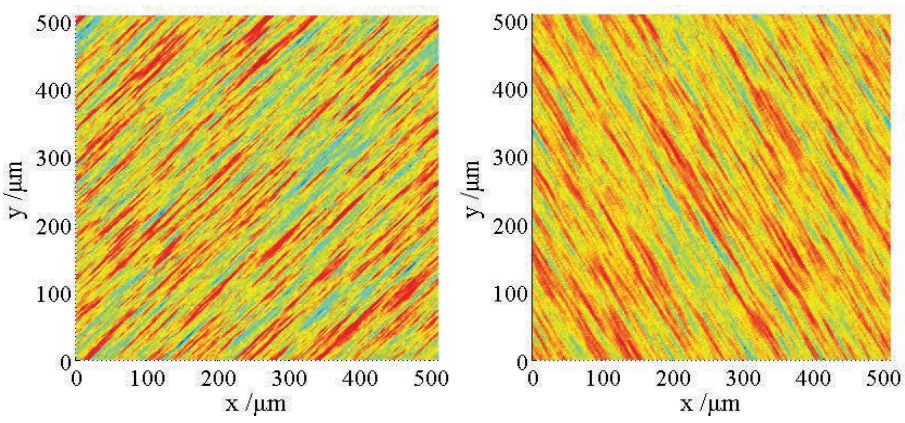

(a) ϕ =45° (b) ϕ =120°

Figure 11: Straight surface texture with different directions.

3 Analysis of contact characteristics of rough interfaces

3.1 Establishment of contact models

Two pairs of Gaussian height sequences generated with the above mentioned methods are utilized to establish two contact models with the application of the corresponding spacing of Δx and Δy in ANSYS. In the two contact models, $\Delta x = \Delta y$=1μm, and the bottom and up contact rough surfaces have the same standard deviation, i.e., σ_1=σ_2, here σ_1=σ_2=1.6 in 1# contact and σ_1=σ_2=0.8 in 2# contact. During the modeling, one of the contact bodies should be turned upside down and translated to be in contact with the other one because of the different normal directions of the two contact rough surfaces.

Besides, some detailed information for modeling is listed as follows:

1. The contact models are established from bottom to up, i.e., from points to rough surfaces to contact bodies which are meshed with Solid45 hexahedral grids.

2. All the contact bodies are supposed to adopt the same material with an elastic modulus of 71GPa and a Poisson's ratio of 0.33;

3. Von Mises plasticity criterion and multi-kinematic hardening rule are introduced with taking the yield strength (σ_s=497Mpa) into consideration;

4. For convenience, the stress-strain curve is defined exactly the same with that in [Oskouei, Keikhosravy and Soutis (2009)].

The constructed contact models are shown in Fig. 12. During the establishment, conta173 and targe170 elements are utilized to model the contact pairs. Afterwards, Solid45 hexahedral elements are adopted to mesh all the contact bodies. In this study, each contact rough surface is simulated with 128×128 points, so the number of solid element which is about 129 thousand ($127\times127\times4\times2$) will be within the calculation ability of common computers and FE software. Moreover, reasonable constraints are applied to improve the solution convergence. Specifically speaking, normal displacement d in z direction, instead of the normal force or pressure, is applied at the top surface of the substrate to adjust the clamping force while the bottom surface of the substrate is fixed. Therefore, only from the reaction force or the contact force at the interface, the corresponding equivalent normal force can be derived.

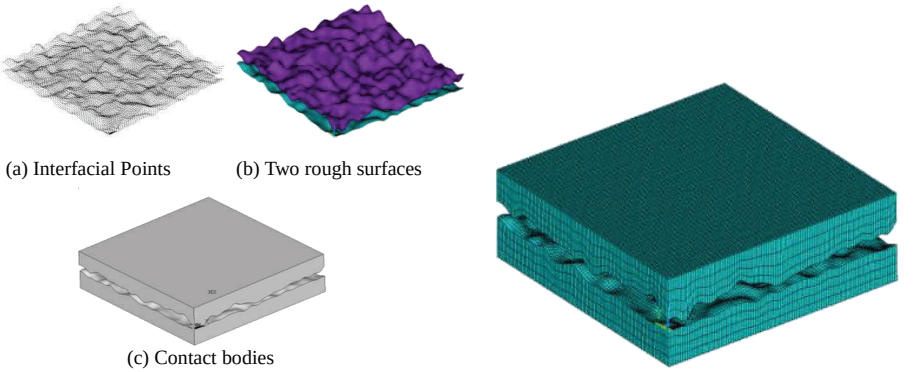

Figure 12: Establishment of the contact model.

3.2 Results and discussion

Using the above established contact models, this section is aimed at revealing the contact characteristics comprised of the load-deformation relationship, the contact pressure distribution, the real contact area and the loading/unloading characteristics at different load levels based on the finite element analysis of 1# and 2# contacts.

3.2.1 Load-deformation relationship

First of all, P_0 is defined as the nominal contact pressure which is equivalent to the quotient of the corresponding contact force F at the interface to the nominal contact area A_0, that is $P_0 = F/A_0$. Then, the elastic-plastic deformation law of rough interface can be elucidated by applying the normal displacement d little by

little from a small value. Meanwhile, through the post-processing of ANSYS, Von Mises equivalent stress σ_e and the corresponding deformation can also be derived. As shown in Fig.13, some asperities show the tendency to yield even under a very small load (P_0=3.44 MPa), and with the increment of P_0 from 3.44 MPa to 141.23 MPa, the asperities yield increasingly from locally to wholly.

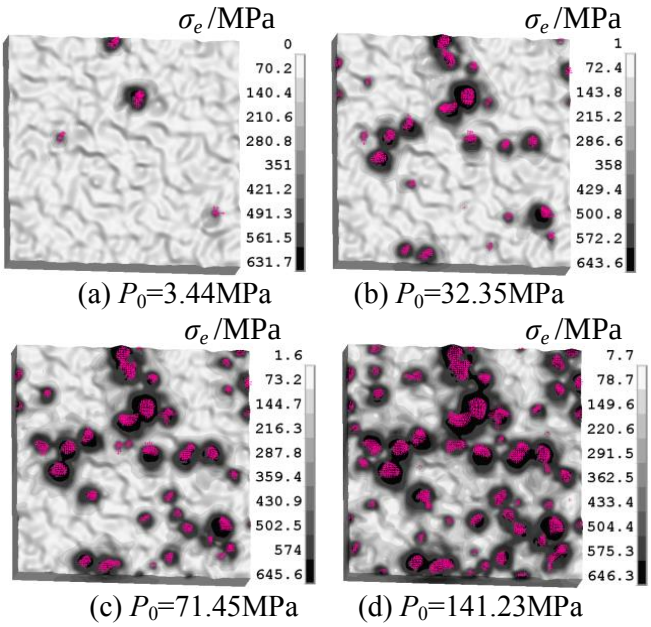

Figure 13: Von Mises equivalent stress of the bottom contact body in 1# contact.

Since the deformation of the thin substrate is so small that could be ignored, the normal deformation of the contact interface is considered to be equal to the normal displacement d. From the data of the normal deformation and the equivalent load P_0, the load-deformation curve can be obtained as shown in Fig.14. It's obvious that under the circumstance of the same normal deformation, the P_0 in 1# contact will be less than that in 2# contact. The slope of the deformation-load curve, enbodying the contact stiffness of the interfaces, increases with P_0 or d, and it changes slowly until P_0 approaches 75MPa. Moreover, under the same load of P_0, the rougher the contact interface, the smaller the slope of the deformation-load curve. Thus, it is verified that the improvement of the sufaces quality and the increment of the assembly load can be beneficial to enhance the contact stiffness.

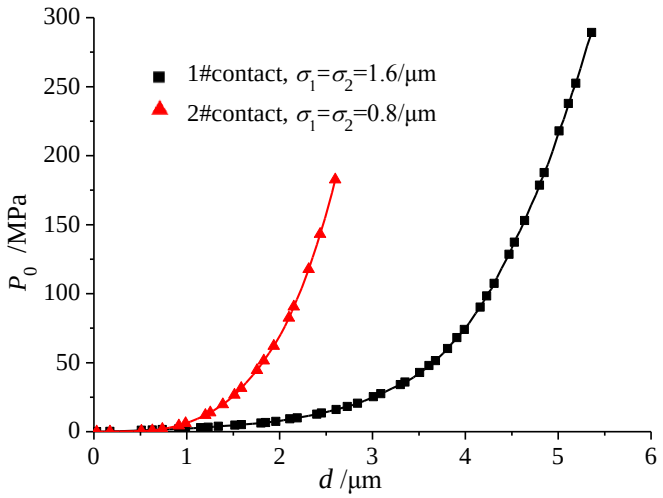

Figure 14: Deformation-load curve of different interfaces.

3.2.2 Interface pressure distribution and real contact area

The interface pressure distribution can also be extracted by the post-processing of ANSYS. As shown in Fig.15, the maximum of contact pressure P is up to 3GPa even under a small normal load of P_0=3.44MPa, and it hardly change with the variation of P_0 from 3.44MPa to 141.23MPa.

The real contact area of the interface is defined as the area with positive contact pressure which can also be obtained from the post-processing of ANSYS. As shown in Fig.16, the ratio of A_r/A_0 of real contact presents a nonlinear increment with the rise of the normal displacement d while a nearly linearly one with the rise of the nominal pressure P_0. When P_0 <100Mpa, the ration of A_r/A_0 is less than 10%, and it is still less than 15% even under a load of P_0=180MPa. Besides, the ratio of A_r/A_0 can also be affected by the roughness of the interface, for example, the ratio of A_r/A_0 in 1# contact is smaller than that in 2# contact.

3.2.3 Loading/unloading characteristics of the contact interfaces

Based on the above analysis of contact characteristics, this section is aimed to reveal the characteristics of interfaces during the loading/unloading processes in the aspect of P_0 and A_r/A_0 as shown in Fig.17 and Fig.18.

As shown in Fig. 17, the interfacial normalized deformation d/σ' is introduced, where $\sigma'=(\sigma_1^2+\sigma_2^2)^{0.5}$. When $d/\sigma' \leq 1.5$, the two loading curves coincide well with each other while P_0 of 2# contact is smaller than that of 1# contact when d/σ'>1.5.

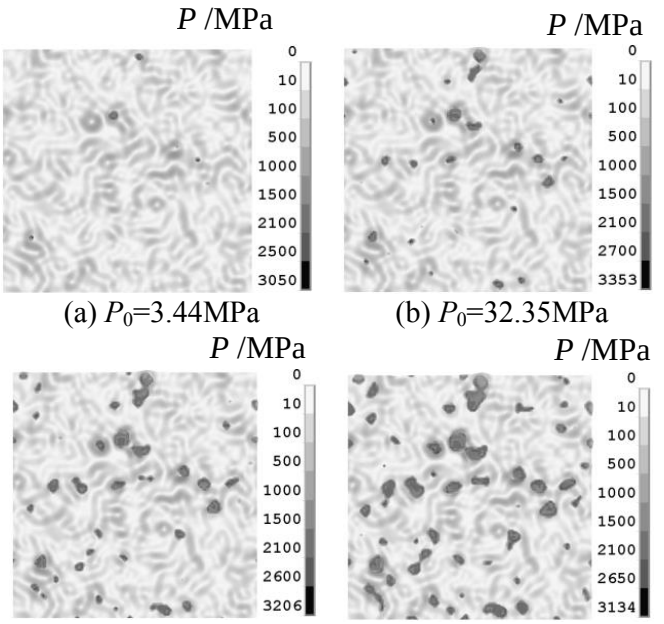

(a) P_0=3.44MPa (b) P_0=32.35MPa

(c) P_0=71.45MPa (d) P_0=141.23MPa

Figure 15: Interface pressure distribution under different load in 1# contact.

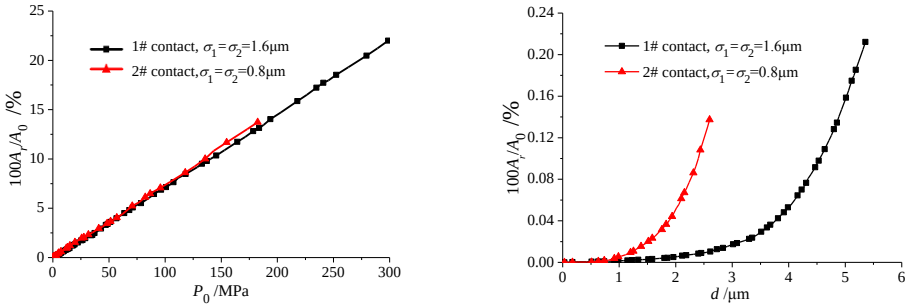

(a) Variation of A_r/A_0 with P_0 (b) Variation of A_r/A_0 with d

Figure 16: variation of A_r/A_0 with the normal load.

Judging from the change of the curve slope, the conclusion that the interface stiffness can be considerably increased by the process of loading and unloading would be reached due to the fact that the slope of unloading curve is obviously larger than that of loading one. Since the characteristics of interfaces during loading and unloading processes in this study is analogous to the deformation-load characteristics

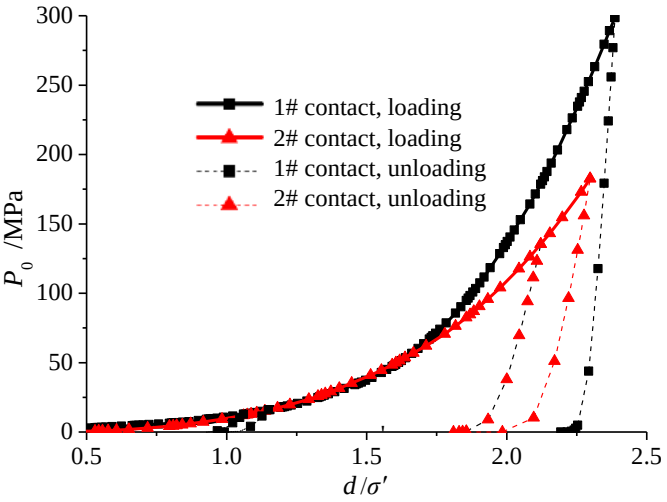

Figure 17: The relationship between d/σ' and P_0 during loading and unloading process.

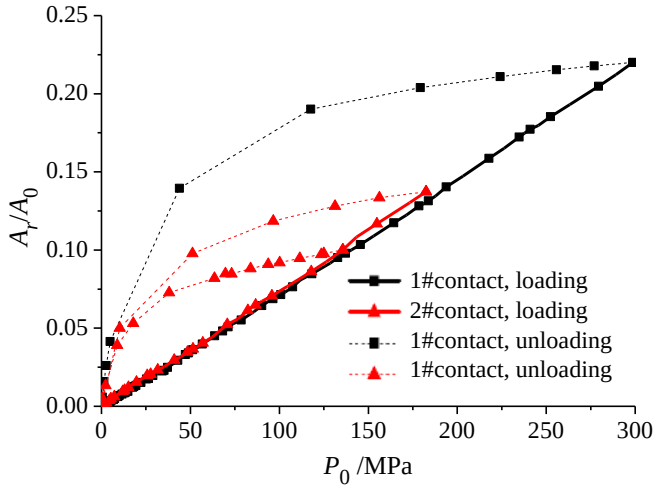

Figure 18: The relationship between A_r/A_0 and P_0 during loading and unloading process.

of the gaskets in [Murali Krishna, Shunmugam and Siva Prasad (2007)], the normal stress, strain and other mechanical behaviors of the interfaces on micro-scale can also be simulated by adopting the gasket elements with a certain thickness to

achieve the cross-scale coupling between micro-scales and macro-scales.

As shown in Fig .18, the ratio of A_r/A_0 of 1# and 2# contact show a linear increment with the rise of P_0 during loading and an apparent non-linear relationship during unloading, which is similar with the results from [Pei, Hyun, Molinari and Robbins (2005)], and thus, verifies the accuracy of the analysis in this study.

4 Conclusions

In this study, a novel scheme is proposed for numerically generating Gaussian and non-Gaussian rough surfaces with isotropic and linear anisotropic surface texture. Afterwards, the contact characteristics including the load-deformation relationship, the contact pressure distribution, the real contact area and the loading/unloading characteristics at different load levels are analyzed. Finally, several conclusions can be drawn as follows:

1. Three-dimensional rough surfaces with any skewness and kurtosis in the whole plane can be numerically generated without complicated linear transformation and filter process of non-Gaussian rough surfaces. Meanwhile, the errors of the skewness and kurtosis obtained from the simulated rough surfaces are less than 0.03 and 0.05, respectively, which is a great improvement compared with the outcome of previous methods

2. Phase sequences are produced from white noises sequences with higher calculation efficiency due to the application of FFT method, and the first four moments of generated Gaussian and non-Gaussian rough surfaces are controlled to closely approach the input ones through the numerical operations like translating, scaling and reconfiguring.

3. The proposed method for generating Gaussian and non-Gaussian rough surfaces would provide massive and accurate surface topography data with different statistical parameters for the study on the contact characteristics of rough surfaces.

4. The simulated models are established by FEM with a high-quality meshing method of hexahedral elements and reasonable constraints which give rise to the improvement of solution accuracy and efficiency. Meanwhile, the contact characteristics including load-deformation relationship, the contact pressure distribution, the real contact area and the interfacial loading/unloading characteristics of rough interfaces are analyzed, which could illuminate the further study of surface topography optimization.

Acknowledgement: This project is supported by the National Natural Science Foundation of China [51405377], the Natural Science Foundation of Hunan Province, China [2015JJ2054], and the Research Foundation of Education Bureau of Hunan Province, China [14C0435].

References

Newland, D. E. (1984): *An Introduction to Random Vibration and Spectral Analysis*. Longman.

Bakolas, V. (2003): Numerical generation of arbitrarily oriented non-Gaussian three-dimensional rough surfaces. *Wear*, vol. 254, pp. 546-554.

Buczkowski, R.; Kleiber, M. (2009): Statistical Models of Rough Surfaces for Finite Element 3D-Contact Analysis. *Arch. Comput. Method. E.*, vol. 16, pp. 399-424.

Chang, W. R.; Etsion, I.; Bogy, D. B. (1987): An Elastic-Plastic Model for the Contact of Rough Surfaces. *J. Tribol.-T ASME*, vol. 109, pp. 257-263.

Chilamakuri, S. K.; Bhushan, B. (1998): Contact analysis of non-Gaussian random surfaces. *P. I. Mech. Eng. J-J. Eng.*, vol. 212, pp. 19-32.

Ciavarella, M.; Greenwood, J. A.; Paggi, M. (2008): Inclusion of "Interaction" in the Greenwood and Williamson Contact Theory. *Wear*, vol. 265, pp. 729-734.

Gao, Y. F.; Bower, A.F.; Kim, K. S.; Lev, L.; Cheng, Y. T. (2006): The Behavior of an Elastic-Perfectly Plastic Sinusoidal Surface under Contact Loading. *Wear*, vol. 261, pp. 145-154.

Greenwood, J. A.; Williams, J. B. (1966): Contact of Nominally Flat Surfaces. *Proc. R. Soc. London, Ser. A*, vol. 295, pp. 300-319.

Hill, I. D.; Hill, R.; Holder, R. L. (1976): Fitting Johnson curves by moments. *Appl. Stat.*, vol. 25, pp. 180-189.

Nagahara, Y. (2003): Non-Gaussian filter and smoother based on the Pearson distribution system. *J. Time Ser. Anal.*, vol. 24, pp. 721-738

Hu, Y. Z.; Tonder, K. (1992): Simulation of 3-D random rough-surface by 2-D digital-filter and Fourier analysis. *Int. J. Mach. Tool. Manu.*, vol. 32, pp. 83-90.

Hyun, S.; Pei, L.; Molinari, J. F.; Robbins, Mark O. (2004): Finite-Element Analysis of Contact between Elastic Self-Affine Surfaces. *Phys. Rev. E*, vol. 70, pp.1-12.

Jackson, R. L.; Green, I. (2005): A Finite Element Study of Elasto-Plastic Hemispherical Contact against a Rigid Flat. *J. Tribol.-T ASME*, vol. 127, pp. 343-354.

Jackson, R. L.; Green, I. (2006): A Statistical Model of Elasto-Plastic Asperity

Contact between Rough Surfaces. *Tribol. Int.*, vol. 39, pp. 906-914.

Majumdar, A.; Bhushan, B. (1991): Fractal Model of Elastic-Plastic Contact between Rough Surfaces. *J. Tribol.-T ASME*, vol. 113, pp. 1-11.

Murali Krishna, M.; Shunmugam, M. S.; Siva Prasad, N. (2007): A study on the sealing performance of bolted flange joints with gaskets using finite element analysis. *Int. J. Pres. Ves. Pip.*, vol. 84, pp. 349-357.

Oskouei, R. H.; Keikhosravy, M.; Soutis, C. (2009): Estimating Clamping Pressure Distribution and Stiffness in Aircraft Bolted Joints by Finite-Element Analysis. *P.I. Mech. Eng. G-J. Aer.*, vol. 223, pp. 863-871.

Patir, N. (1978): A numerical procedure for random generation of rough surfaces. *Wear*, vol. 47, pp. 263-277

Pei, L.; Hyun, S.; Molinari, J. F.; Robbins, M. O. (2005): Finite element modeling of elasto-plastic contact between rough surfaces. *J. Mech. Phys. Solids*, vol. 53, no. 11, pp. 2385-2409.

Reizer, R. (2011): Simulation of 3D Gaussian surface topography. *Wear*, vol. 271, pp. 539-543.

Sahoo, P.; Ghosh, N. (2007): Finite Element Contact Analysis of Fractal Surfaces. *J. Phys. D: Appl. Phys.*, vol. 40, pp. 4245-4252.

Seong, S. H.; Peterka, J. A. (1997): Computer simulation of non-Gaussian multiple wind pressure time series. *J. Wind Eng. Ind. Aerod.*, vol. 72, pp. 95-105.

Suresh Kumar, K.; Stathopoulos, T. (1999): Synthesis of non-Gaussian wind pressure time series on low building roofs. *Eng. Struct.*, vol. 21, pp. 1086-1100.

Watson, W.; King, T. G.; Spedding, T. A.; Stout, K. J. (1979): The machined surface—time series modeling. *Wear*, vol. 57, pp. 195-205.

Watson, W.; Soedding, T. A. (1982): The time series modelling of non-Gaussian engineering processes. *Wear*, vol. 83, pp. 215-231.

Wu, J. J. (2000): Simulation of rough surfaces with FFT. *Tribol. Int.*, vol. 33, pp. 47-58.

Wu, J. J. (2004): Simulation of non-Gaussian surfaces with FFT. *Tribol. Int.*, vol. 37, pp. 339-346.

Yu, N.; Polycarpou, A. A. (2004): Combining and Contacting of Two Rough Surfaces with Asymmetric Distribution of Asperity Heights. *J. Tribol.-T ASME*, vol. 126, pp. 225-232.

Zhao, Y. W.; Chang, L. (2001): A Model of Asperity Interactions in Elastic-Plastic Contact of Rough Surfaces. *J. Tribol.-T ASME*, vol. 123, pp. 857-864.